Electronic Supplementary Material (ESI) for Journal of Materials Chemistry A.

Supporting Information

Coupling Doped Halogen Sites Copper(I)-Organic Frameworks with Cuprous Oxide for High Selectivity CO_2 Photoreduction with H_2O

Jing Liang,[a]+ Shengfu Huang,[a]+ Yuan Chang,[b]+ Andreas Terfort,[c] Junfeng Gao,*[b] and Jinxuan Liu*[a]

[a] State Key Laboratory of Fine Chemicals, Dalian University of Technology, 116024 Dalian, P. R. China.

E-mail: Jinxuan.liu@dlut.edu.cn

[b] Laboratory of Materials Modification by Laser, Ion and Electron Beams, Ministry of Education, Dalian University of Technology, 116024 Dalian, P. R. China.

E-mail: gaojf@dlut.edu.cn

[c] Department of Chemistry, Institute of Inorganic and Analytical Chemistry, Goethe University Frankfurt, Max-von-Laue-Street 7, 60438 Frankfurt, Germany.

Experimental Details

Material

Chemicals used in this paper are commercially available and used as received without further purification. $CuSO_4 \cdot 5H_2O$, sodium citrate, NaOH, ascorbic acid, cuprous chloride, cuprous bromide, cuprous iodide, 4,4'-bipyridine and acetonitrile were bought from Aladdin. Deionized water (DI) used in the synthesis process was obtained from local sources.

Synthesis of Cu_2O nanocubes

The Cu_2O nanocubes are synthesized according to the previously reported approach with slight modification.[1] In a typical synthesis, $CuSO_4 \cdot 5H_2O$ (4.5 mmol) and sodium citrate (1.5 mmol) were dissolved into 240 mL of deionized water with stirring for 10 min. Then, 60 mL of 1.25 M NaOH was added to the above solution under stirring. After 10 min, 150 mL of 0.03 M ascorbic acid was added to the suspension under stirring for 5 min. The obtained mixed solution was aged for 1 hour at room temperature. The precipitate was collected by centrifugation, and washed with DI and ethanol three times, followed by drying under vacuum at 60 ℃ for 12 h.

Synthesis of Cu_2O@CuCl-bpy

Cu_2O nanocubes (20 mg) and 4,4'-bipyridine (8 mg) were first dispersed into 5 mL of acetonitrile and cuprous chloride (5 mg) was dispersed into 1 mL of acetonitrile. After that, the solution was both sonicated for 30 min. Then, the above solution was mixed under stirring. After ultrasound for 1 hour, the precipitate was collected by centrifugation, washed with DI and ethanol three times, and followed by drying under vacuum at 60 ℃ for 12 h.

Synthesis of Cu_2O@CuBr-bpy / Cu_2O@CuI-bpy

Cu_2O@CuBr-bpy/Cu_2O@CuI-bpy was prepared by the above method for Cu_2O@CuCl-

bpy except that cuprous chloride was replaced by cuprous bromide (7.2 mg) / cuprous iodide (9.5 mg).

Characterizations

Power X-ray diffraction (XRD) data were collected in Bragg-Brettano mode in the 2θ range from 5° to 80° at a scan rate of 10° min^{-1} on a Rigaku Dmax-2000 diffractometer operating at a voltage of 40 kV using Cu Kα radiation (λ = 1.5405 Å). SEM images were captured by a field-emission scanning electron microscope (Nova Nano SEM 450). The chemical states and chemical composition of the products were determined by X-ray photoelectron spectra (XPS) in Thermo ESCALAB XI. The shift of binding energy due to relative surface charging was corrected using the C 1 s level at 284.8 eV as an internal standard. The optical properties of the products were analyzed by ultraviolet-visible (UV-vis) absorption spectroscopy using a UV-vis spectrophotometer (Shimadzu UV-3600 Plus). The photocurrent response (I-t), Open-circuit potential decay curves (OCP) and electrochemical impedance spectroscopy (EIS) experiments were conducted on CHI760E electrochemical workstation. The photoluminescence tests (PL) of the products were obtained by fluorescence spectroscopy (FloroMax-4P) at room temperature. Time-resolved photoluminescence measurements of the products were conducted at room temperature by FLS1000.

Photoelectrochemical measurements

The photoelectrochemical (PEC) measurements were performed on a CHI760E electrochemical workstation equipped with the three-electrode cell. Firstly, the original FTO glasses were cleaned with acetone, ethanol and DI water. The working electrode was coated with a glass FTO electrode with the catalyst, dipcoating the electrode in a slurry consisting

of 5 mg photocatalyst and 1 mL DI water. The counter electrode was a platinum foil, the reference electrode was a saturated Ag/AgCl electrode, and the electrolyte was 0.2 M Na_2SO_4. The light source was a 300W Xe lamp with a light intensity of about 200 mW cm^{-2}. The I-t curves were measured without bias voltage. The electrochemical impedance spectroscopy (EIS) measurements were conducted over a frequency range of 0.01-10^5 Hz. Mott-Schottky plots of photocatalysts with the same three-electrode system were obtained under frequencies of 500, 1000, 1500, 2000 and 3000 Hz.

In-situ FTIR measurements

In-situ FTIR spectra were obtained by using a VERTEX 80v, equipped with an MCT detector cooled by liquid nitrogen. In detail, as for CO_2 photoreduction, the sample was degassed in CO_2 atmosphere for 30 min at room temperature. The background spectrum was collected after 30 min of adsorption in Saturated CO_2 aqueous solution. After turning on the light, in-situ FTIR spectra were recorded continually for 30 min, averaging 32 scans at a 2 cm^{-1} spectral resolution.

Photoactivity testing

To evaluate the photocatalytic activity of the photocatalyst, photocatalytic CO_2 reduction was conducted using the synthesized photocatalyst (2 mg) in a Quartzose vessel (40 mL) containing 5 mL DI. Further, the vessel was sonicated for 20 minutes to disperse the photocatalyst in solution. CO_2 (purity: 99.999%) was introduced to the reactor with a flow rate of 20 cm^3/min for 30 minutes to saturate the solution. After that, a 300 W Xe lamp (light intensity: 200 mW·cm^{-2}) with a 400 nm high-pass filter was used as the light source for the photocatalytic reactions, the reaction system was vigorously stirred with a magnetic stirrer and a mild reaction temperature of 25 ℃ was maintained by a circulation cooling water. The

gas products (O_2 and other possible products) in the headspace of the reactor were collected through a syringe and analyzed via the gas chromatograph (GC, Techcomp 7900), equipped with TCD and FID detectors. The liquid products (HCOOH and other possible CO_2 reduction products) in the solution were centrifuged to remove the photocatalyst after photocatalysis, and the supernat was analyzed by Ion Chromatography (IC, CIC-D100).

Computational Methods

We employ VASP 6.3.0 code[2, 3] to implement density functional theory (DFT) calculations. The exchange and correlation interaction isdescribed by the Perdew-Burke-Ernzerhof (PBE) method[4] of generalized gradient approximation (GGA) functional. The Van der Waals interaction is handled by empirical DFT-D3 (BJ) correction[5, 6] due to the existence of C, O, H and halogenated elements. Spin-polarization is released. The cutoff energy is set to be 500 eV. An adequate gamma-centered 1×1×1 k-mesh is utilized for optimization due to the large cell. The criteria of energy convergence and force convergence are set to 10^{-5} eV and 0.01 eV/ Å. All the numerical accuracy has been carefully tested. During self-consistent field calculations, the following valence electrons were induced: H ($1s^1$), C ($2s^2$ and $2p^2$), O ($2s^2$ and $2p^4$), Cl ($3s^2$ and $3p^5$), Br ($4s^2$ and $4p^5$) and I ($5s^2$ and $5p^5$).

OER Mechanism

The process of OER can be described as following relations (Adsorbates evolution mechanism):

$$^*OH + OH^- \rightarrow {}^*O + H_2O + e^- \quad (1)$$

$$^*O + OH^- \rightarrow {}^*OOH + e^- \quad (2)$$

$$^*OOH + OH^- \rightarrow {}^*OO + H_2O + e^- \quad (3)$$

$$^*OO + OH^- \rightarrow O_2 + {}^*OH + e^- \quad (4)$$

According to above equations, free energy of different absorption could be obtained by the equation

$$E_{a(^*OH)} = E_{^*OH} - E_{^*} - \left(E_{H_2O} - \frac{1}{2}E_{H_2}\right) \quad (5)$$

$$E_{a(^*O)} = E_{^*O} - E_{^*} - \left(E_{H_2O} - E_{H_2}\right) \quad (6)$$

$$E_{a(^*OOH)} = E_{^*OOH} - E_{^*} - \left(2E_{H_2O} - \frac{3}{2}E_{H_2}\right) \quad (7)$$

$$\Delta G = E_{ads} + \Delta E_{ZPE} - T\Delta S \quad (8)$$

where ΔE_{ZPE} represents the vibrations of all degrees of freedom of adsorbates under the harmonic approximation, T and ΔS are temperature and entropy change. Next, the free energy corresponding to each step could be calculated

$$\Delta G_1 = \Delta G_{^*OH} \quad (9)$$

$$\Delta G_2 = \Delta G_{^*O} - \Delta G_{^*OH} \quad (10)$$

$$\Delta G_3 = \Delta G_{^*OOH} - \Delta G_{^*O} \quad (11)$$

$$\Delta G_4 = 4.92 - \Delta G_{^*OOH} \quad (12)$$

$$G^{OER} = \max\left\{\Delta G_1, \Delta G_2, \Delta G_3, \Delta G_4\right\} \quad (13)$$

$$\eta^t = G^{OER}/e - 1.23\ V \quad (14)$$

where G^{OER} represents the free energy of OER while η^t is the required overvoltage for oxygen evolution.

As for Cu_2O which contains lattice oxygen, the lattice oxygen oxidation (LOM) mechanism is probably more favored than the adsorbates evolution (AEM) mechanism. A diagram of these two mechanisms is given in **Figure S15**. In this case, free energy of different absorption could be obtained by the equation

$$E_{a(^*OO+O_V)} = E_{^*OO+O_V} - E_{^*} - (E_{H_2O} - E_{H^2}) \quad (15)$$

$$E_{a(^*OH+\ ^*OO+O_V)} = E_{^*OH+\ ^*OO+O_V} - E_{^*} - (2E_{H_2O} - \frac{3}{2}E_{H^2}) \quad (16)$$

$$E_{a(^*OH+O_V)} = E_{^*OH+O_V} - E_{^*} - \frac{1}{2}E_{H_2} \quad (17)$$

$$E_{a(^*OH+\ ^*OH+O_V)} = E_{^*OH+\ ^*OH+O_V} - E_{^*} - E_{H_2O} \quad (18)$$

Free energy is obtained by equation (8). Next, the free energy corresponding to each step could be calculated

$$\Delta G_1 = \Delta G_{*OH} - \Delta G_{*OH + *OH + O_V} \quad (19)$$

$$\Delta G_2 = \Delta G_{*OO + O_V} - \Delta G_{*OH} \quad (20)$$

$$\Delta G_3 = \Delta G_{*OH + *OO + O_V} - \Delta G_{*OO + O_V} \quad (21)$$

$$\Delta G_4 = 4.92 - \Delta G_{*OH + *OO + O_V} \quad (22)$$

$$\Delta G_5 = \Delta G_{*OH + *OH + O_V} - \Delta G_{*OH + O_V} \quad (23)$$

$$G^{OER} = \max\{\Delta G_1, \Delta G_2, \Delta G_3, \Delta G_4, \Delta G_5\} \quad (24)$$

CO_2RR Mechanism

The process of CO_2RR can be described as following relations to form formic acid (FA) or carbon monoxide (CO):

Formic acid (FA) pathway

$$CO_2(g) + e^- + H^+ + * \rightarrow {}^*OCHO \quad (25)$$

$${}^*OCHO + e^- + H^+ \rightarrow {}^*HCOOH \quad (26)$$

$${}^*HCOOH \rightarrow HCOOH(aq) + * \quad (27)$$

Carbon monoxide (CO) pathway

$$CO_2(g) + e^- + H^+ + * \rightarrow {}^*COOH \quad (28)$$

$${}^*COOH + e^- + H^+ \rightarrow {}^*CO + H_2O \quad (29)$$

$${}^*CO \rightarrow CO(g) + * \quad (30)$$

The difference between the two pathways is the adsorption tendency of hydrogen atoms. After $*CO_2$ intermediate adsorption, if the hydrogen atom prefers to be adsorbed at carbon atom, then the reaction comes to FA pathway, otherwise, it is CO pathway.

In FA pathway, free energy of different absorption could be obtained by the equation

$$E_{a({}^*CO_2)} = E_{*CO_2} - E_* - E_{CO_2} \quad (31)$$

$$E_{a({}^*OCHO)} = E_{*OCHO} - E_* - (E_{HCOOH} - \frac{1}{2}E_{H^2}) \quad (32)$$

The same as OER process, free energy is obtained by equation (8). Next the free energy corresponding to each step could be calculated

$$\Delta G_1 = \Delta G_{*CO_2} \tag{33}$$

$$\Delta G_2 = \Delta G_{*OCHO} - \Delta G_{*CO_2} \tag{34}$$

$$\Delta G_3 = -\Delta G_{*OCHO} \tag{35}$$

$$G^{CO_2 RR} = \max\{\Delta G_1, \Delta G_2, \Delta G_3\} \tag{36}$$

Figures and Tables

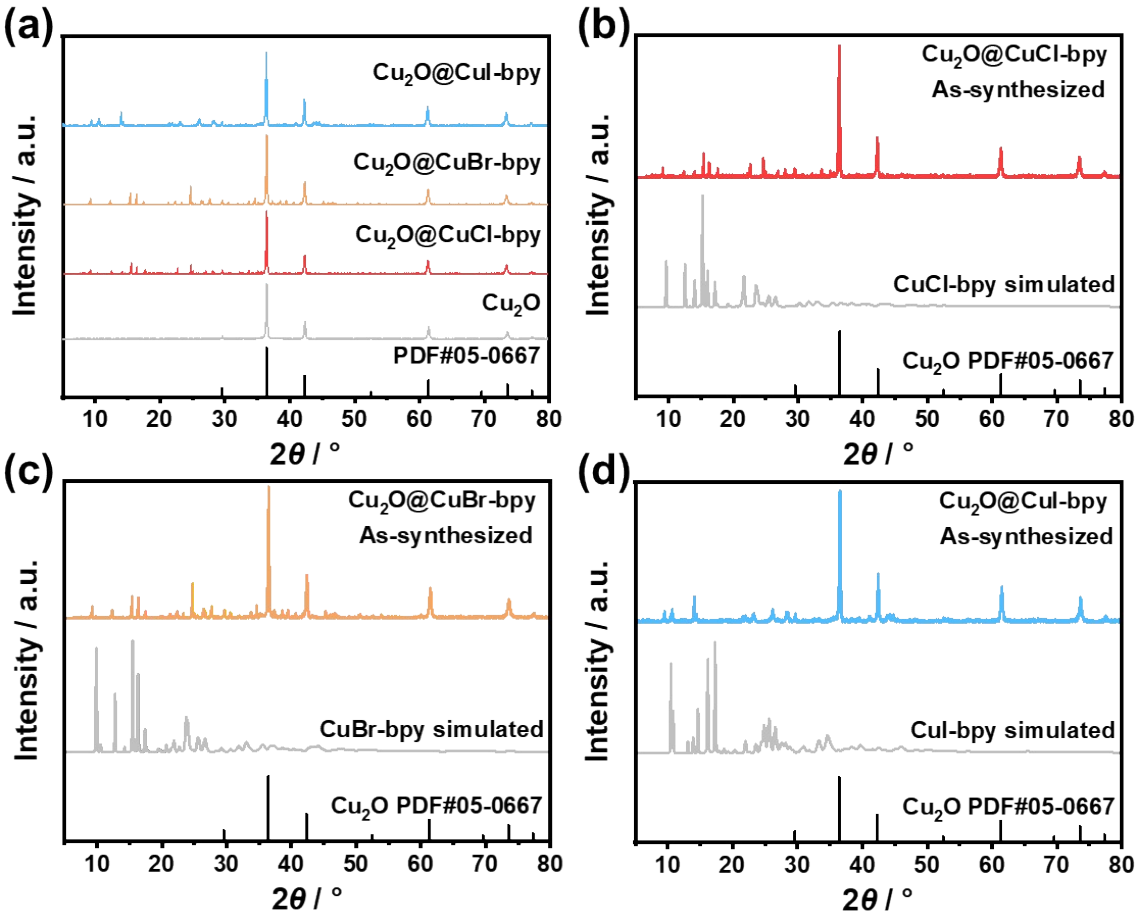

Figure S1. PXRD patterns of (a) Cu_2O nanocubes and Cu_2O@CuX-bpy, (b) Cu_2O@CuCl-bpy, (c) Cu_2O@CuBr-bpy and (d) Cu_2O@CuI-bpy.

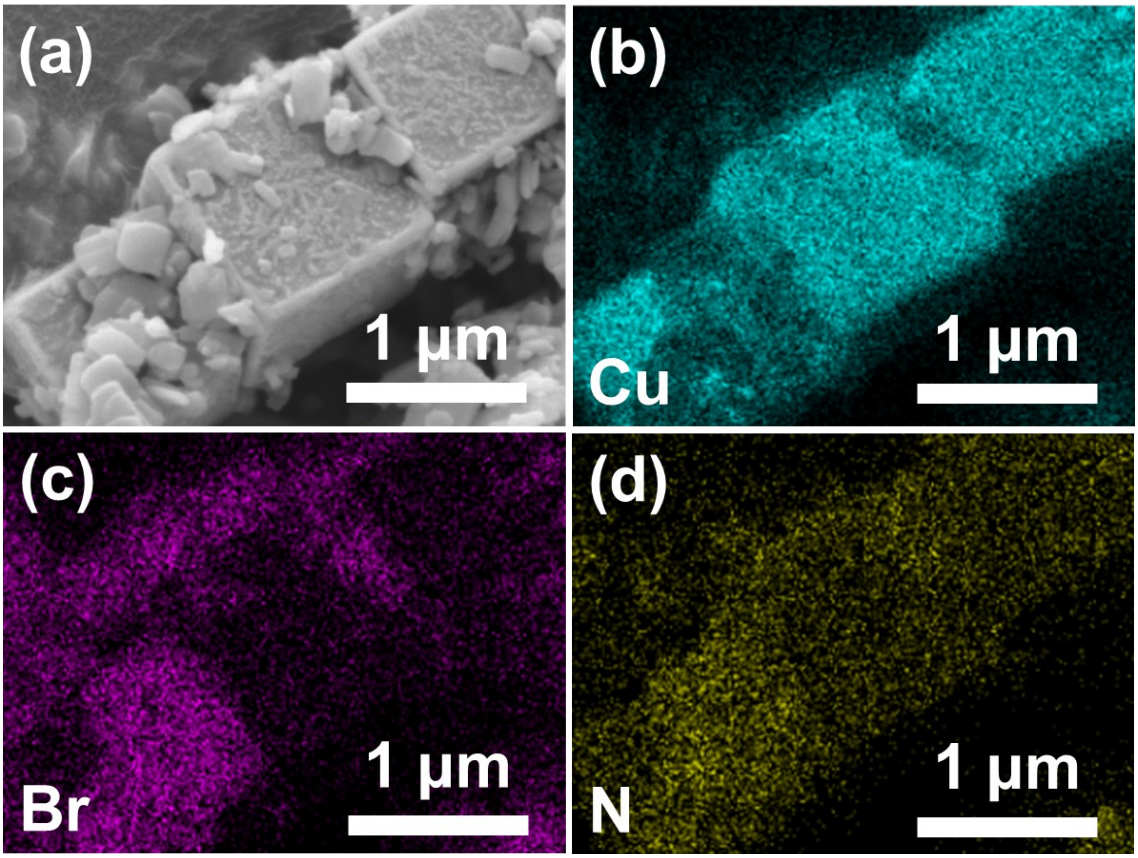

Figure S2. SEM images of the Cu_2O@CuBr-bpy and its corresponding element mapping images of Cu, Br, N.

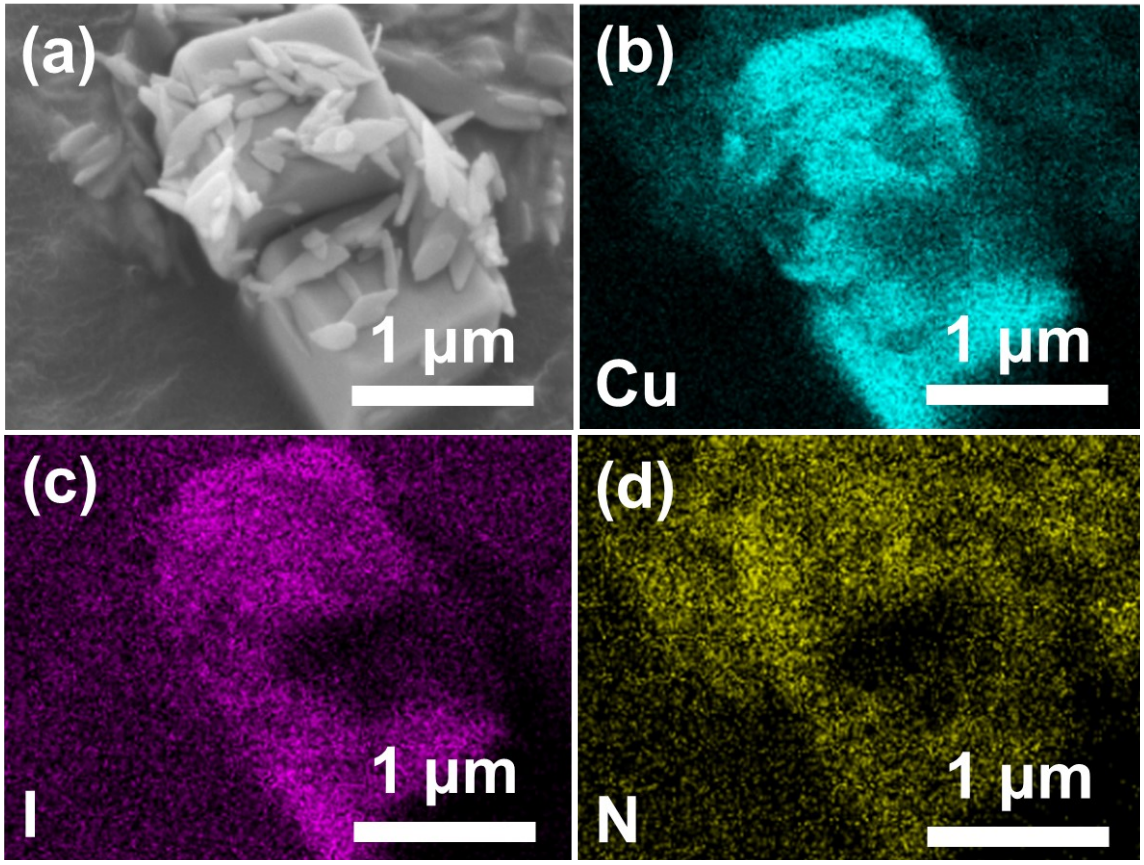

Figure S3. SEM images of the Cu_2O@CuI-bpy and its corresponding element mapping images of Cu, I, N.

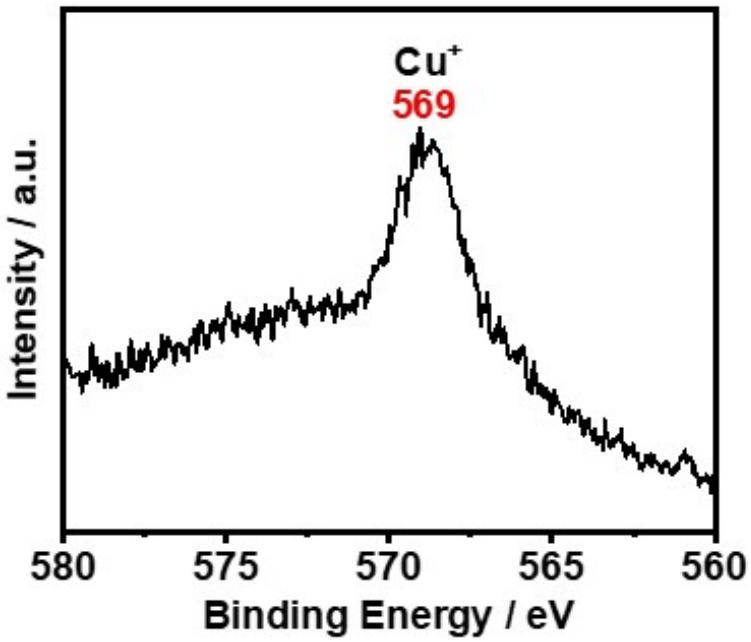

Figure S4. Cu LMM Auger spectrum of the Cu_2O@CuI-bpy.

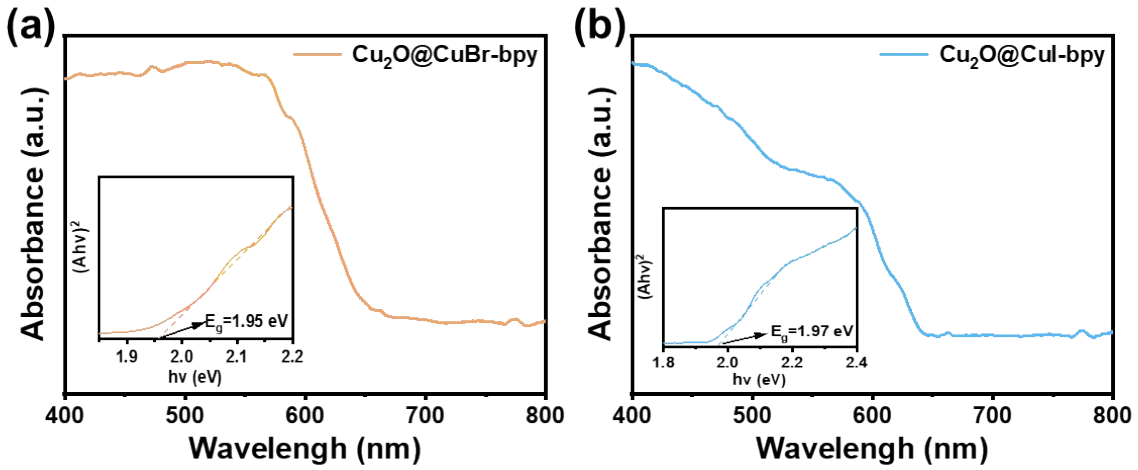

Figure S5. UV-vis DRS spectra (inset: tauc plots) of (a) Cu_2O@CuBr-bpy and (b) Cu_2O@CuI-bpy.

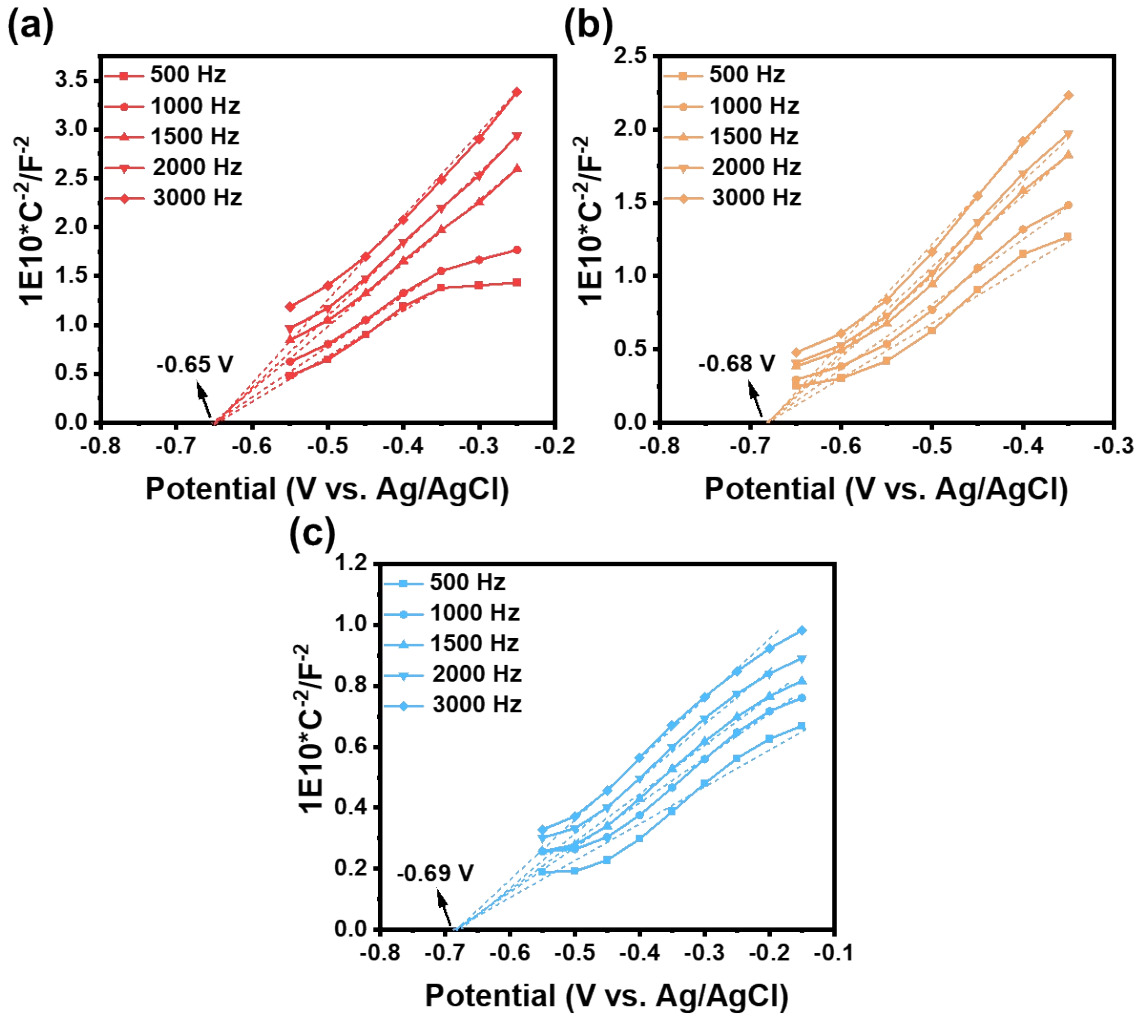

Figure S6. Mott-Schottky curves of (a) Cu_2O@CuCl-bpy, (b) Cu_2O@CuBr-bpy and (c) Cu_2O@CuI-bpy.

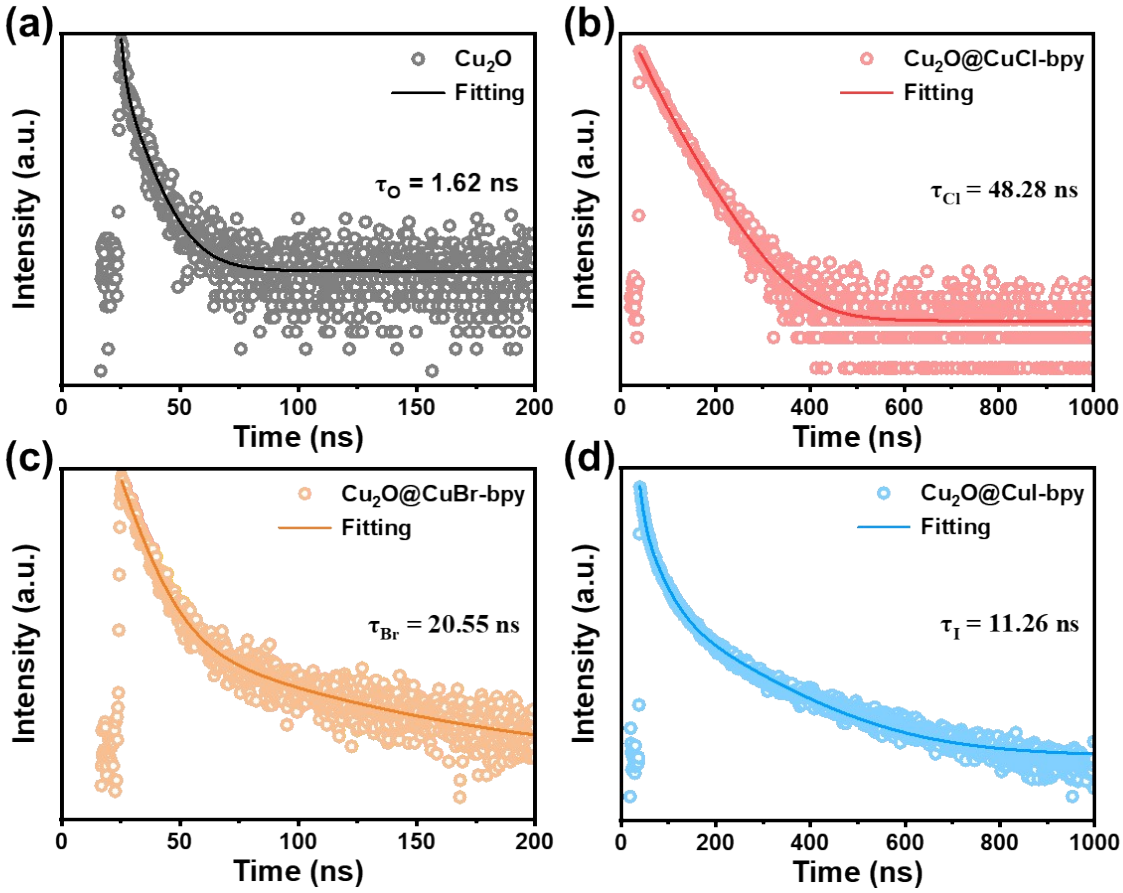

Figure S7. Time-resolved PL spectra of (a) Cu_2O, (b) Cu_2O@CuCl-bpy, (c) Cu_2O@CuBr-bpy and (d) Cu_2O@CuI-bpy.

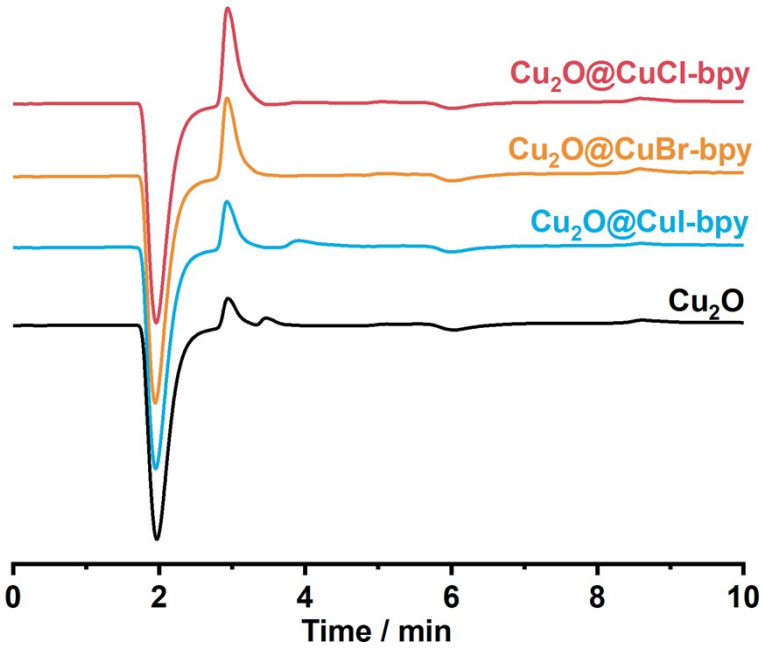

Figure S8. Ion chromatograph of Cu_2O, Cu_2O@CuX-bpy (X = Cl, Br and I).

It shows HCOOH was the main ion production.

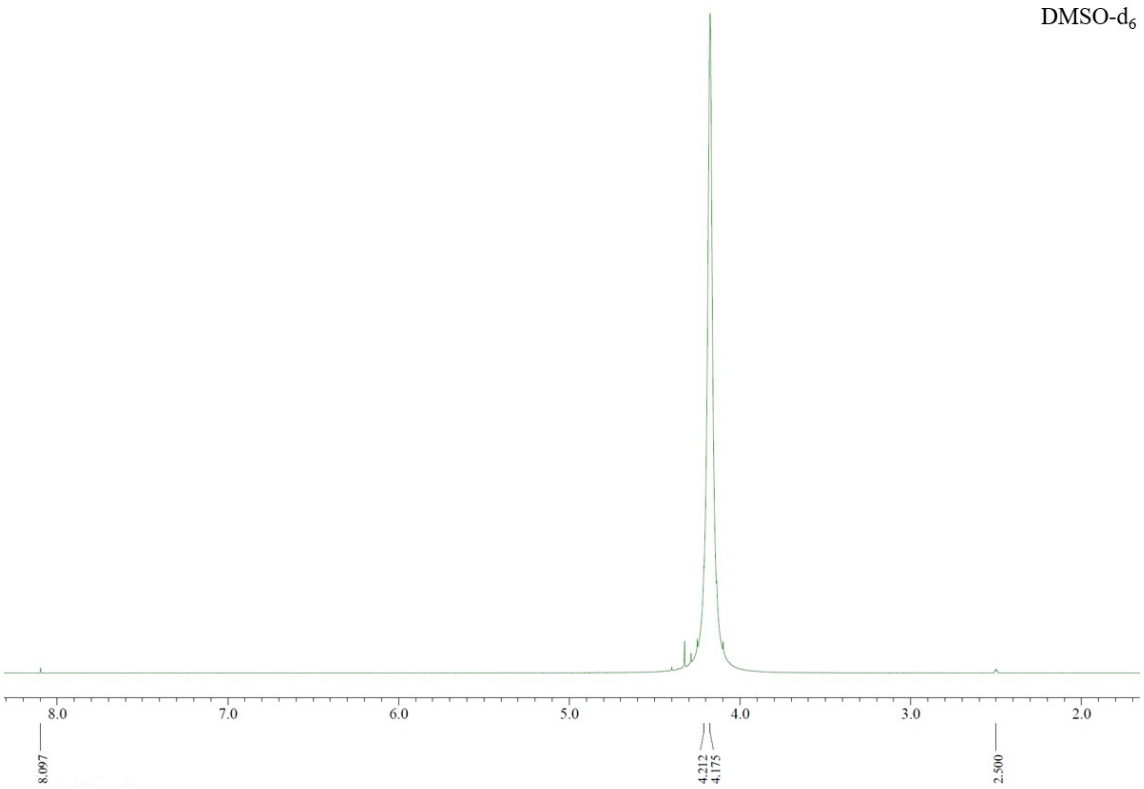

Figure S9. 1H NMR spectra for the filtrate after 12-h photocatalytic reaction.

The catalyst was isolated by filtration, and NMR was conducted on the filtrate. The NMR spectrum (Figure S8) indicates no other organic molecules detected but HCOOH.

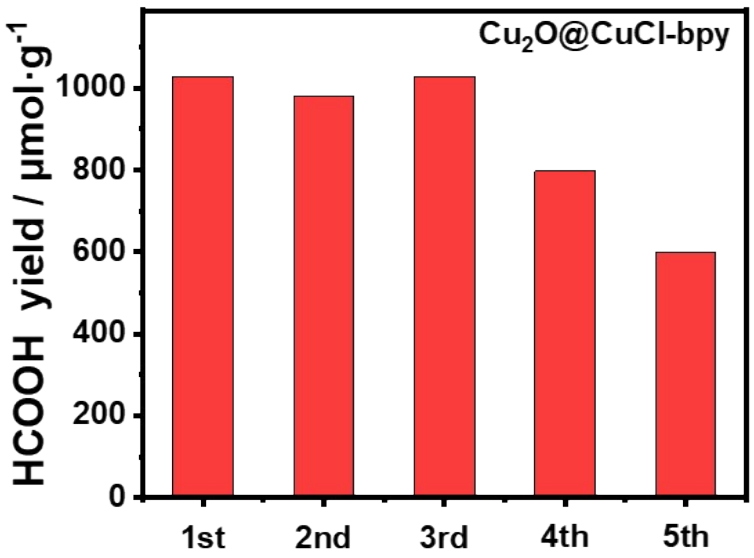

Figure S10. Stability test of Cu_2O@CuCl-bpy in the reaction system (6 h test per cycle).

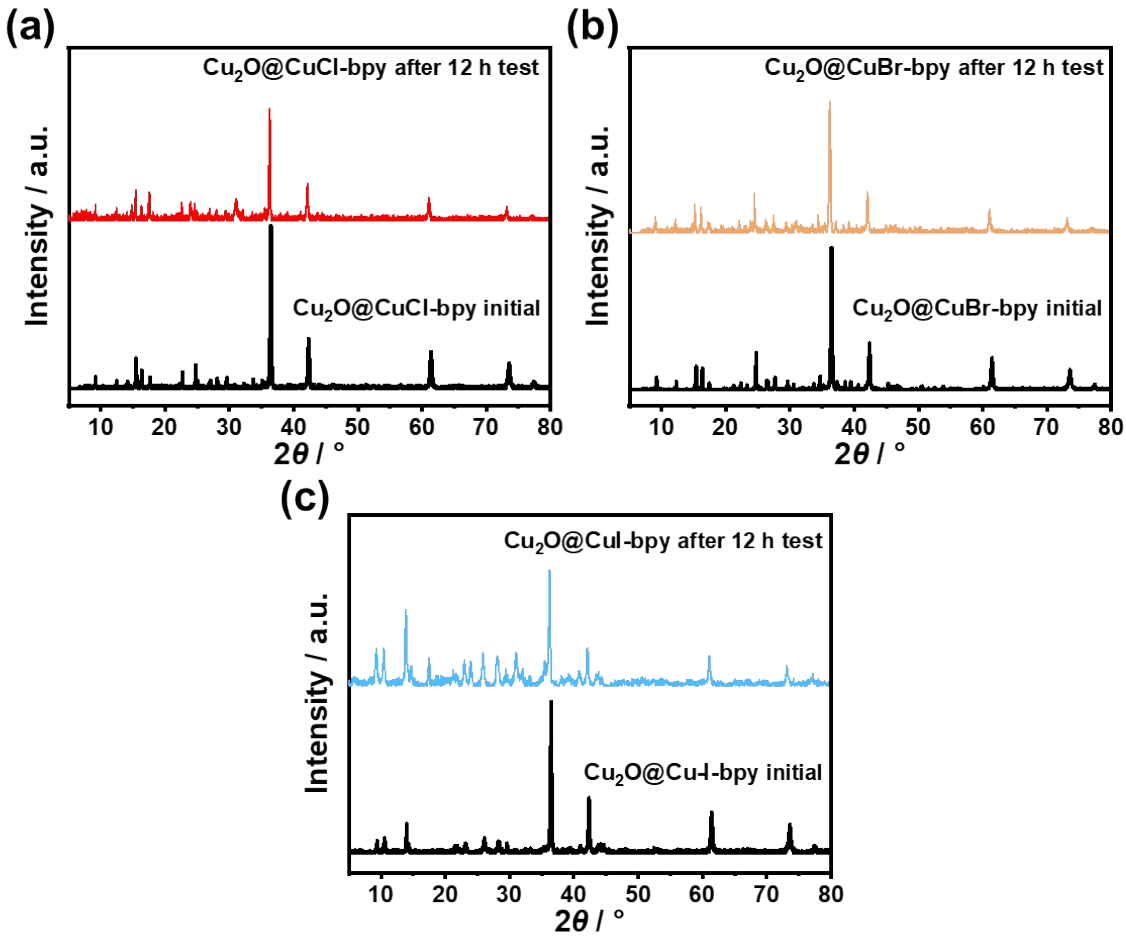

Figure S11. PXRD patterns of initial Cu_2O@CuX-bpy and Cu_2O@CuX-bpy after 12 h photocatalysis.

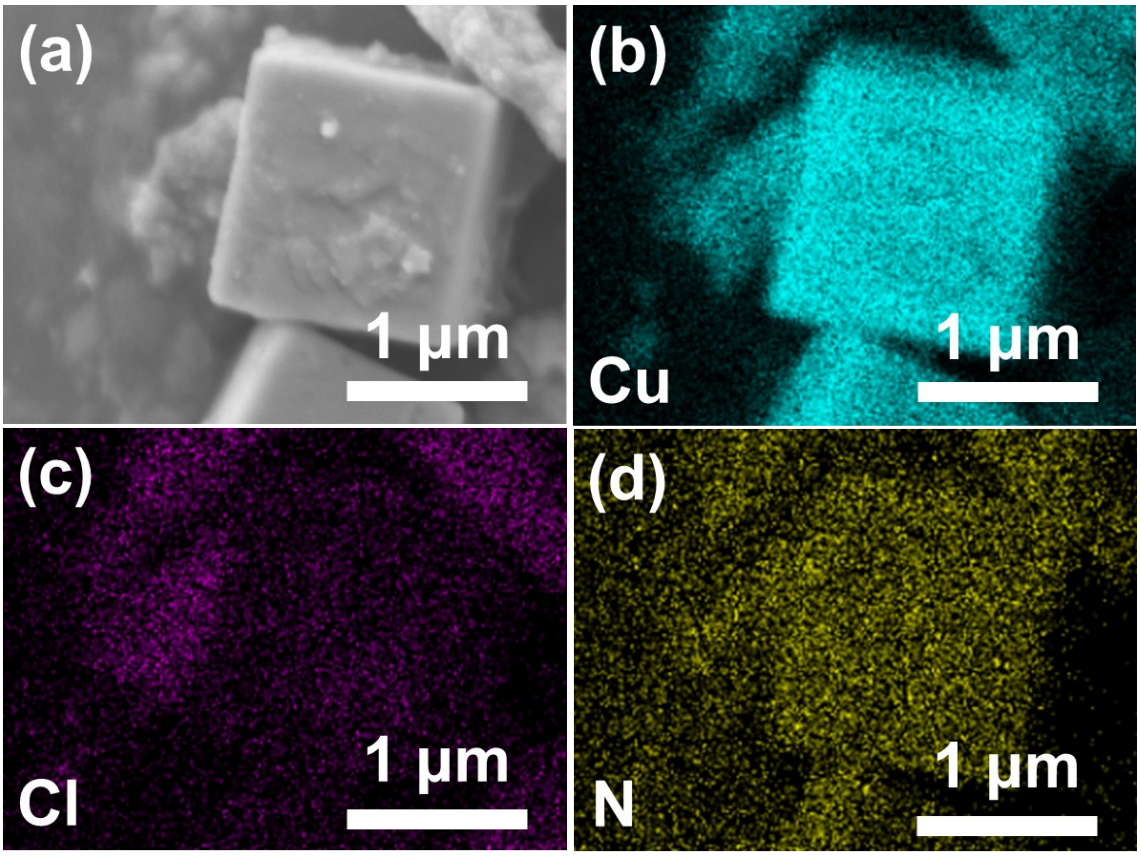

Figure S12. SEM images of the Cu_2O@CuCl-bpy after 12 h photocatalysis and its corresponding element mapping images of Cu, Cl, N.

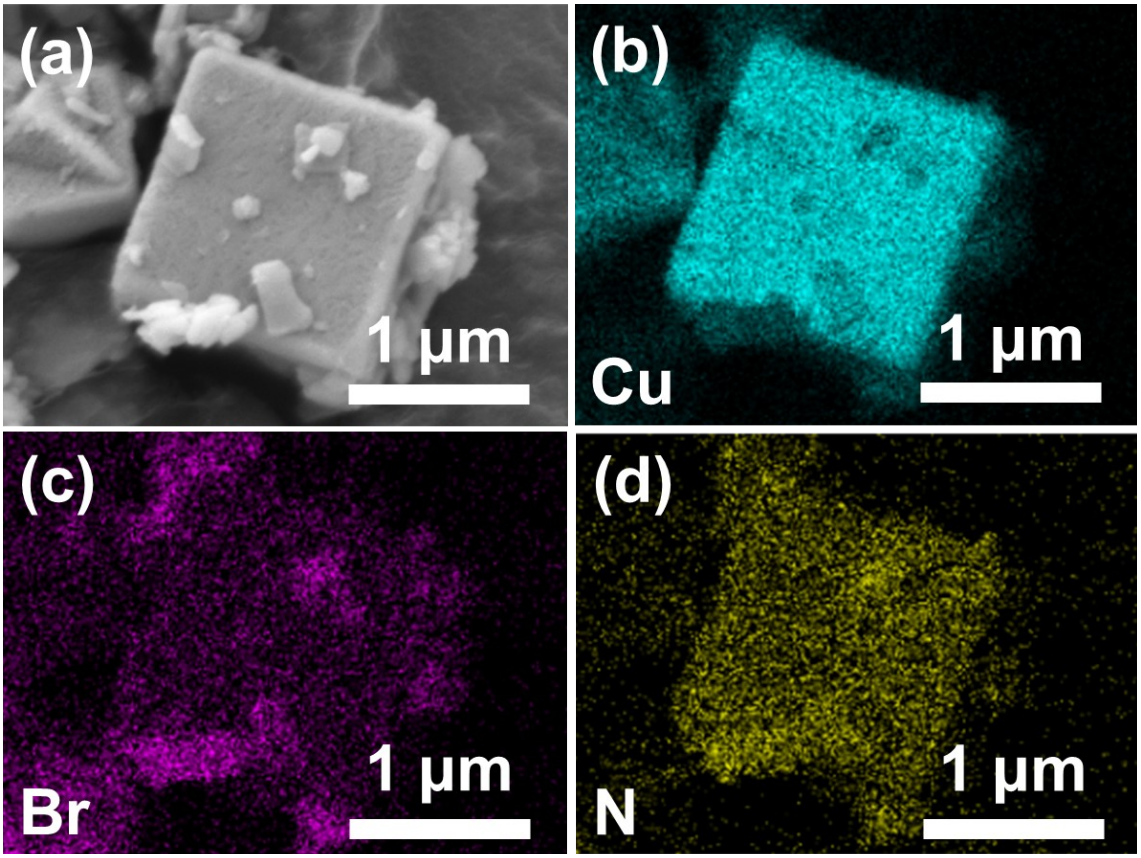

Figure S13. SEM images of the Cu_2O@CuBr-bpy after 12 h photocatalysis and its corresponding element mapping images of Cu, Br, N.

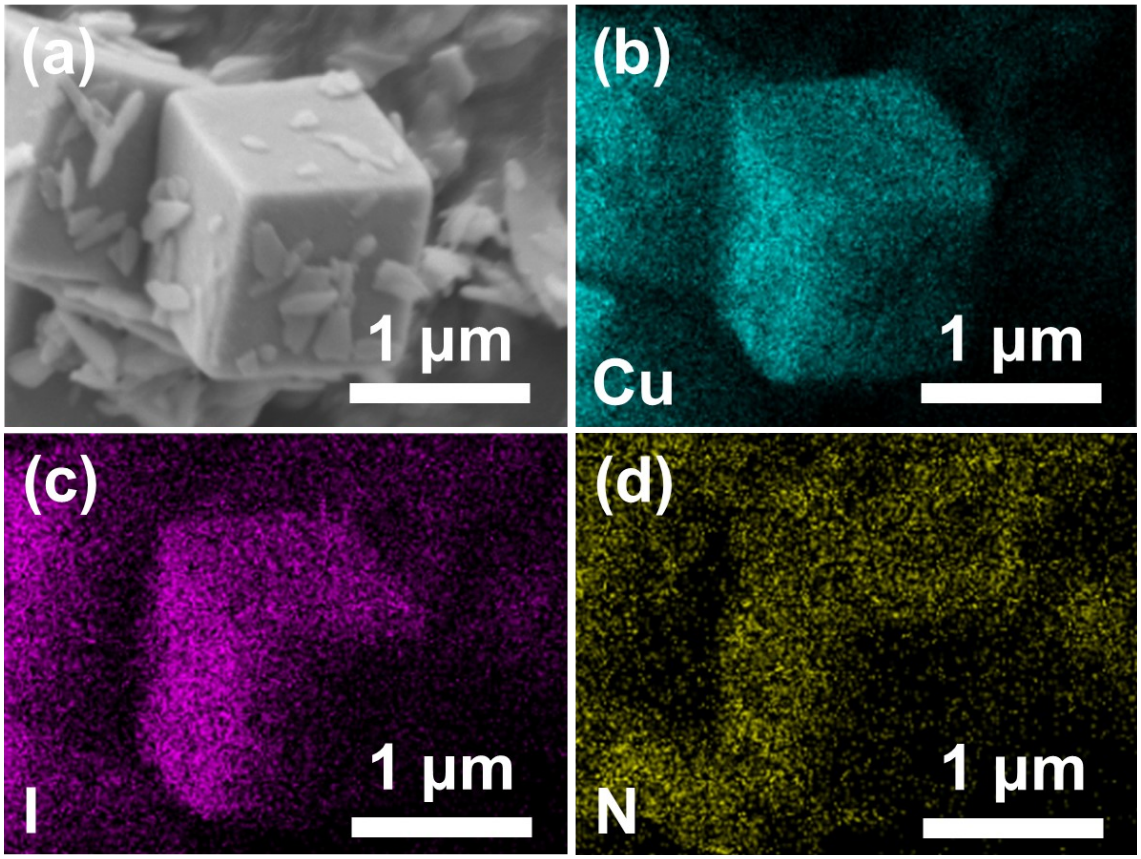

Figure S14. SEM images of the Cu_2O@CuI-bpy after 12 h photocatalysis and its corresponding element mapping images of Cu, I, N.

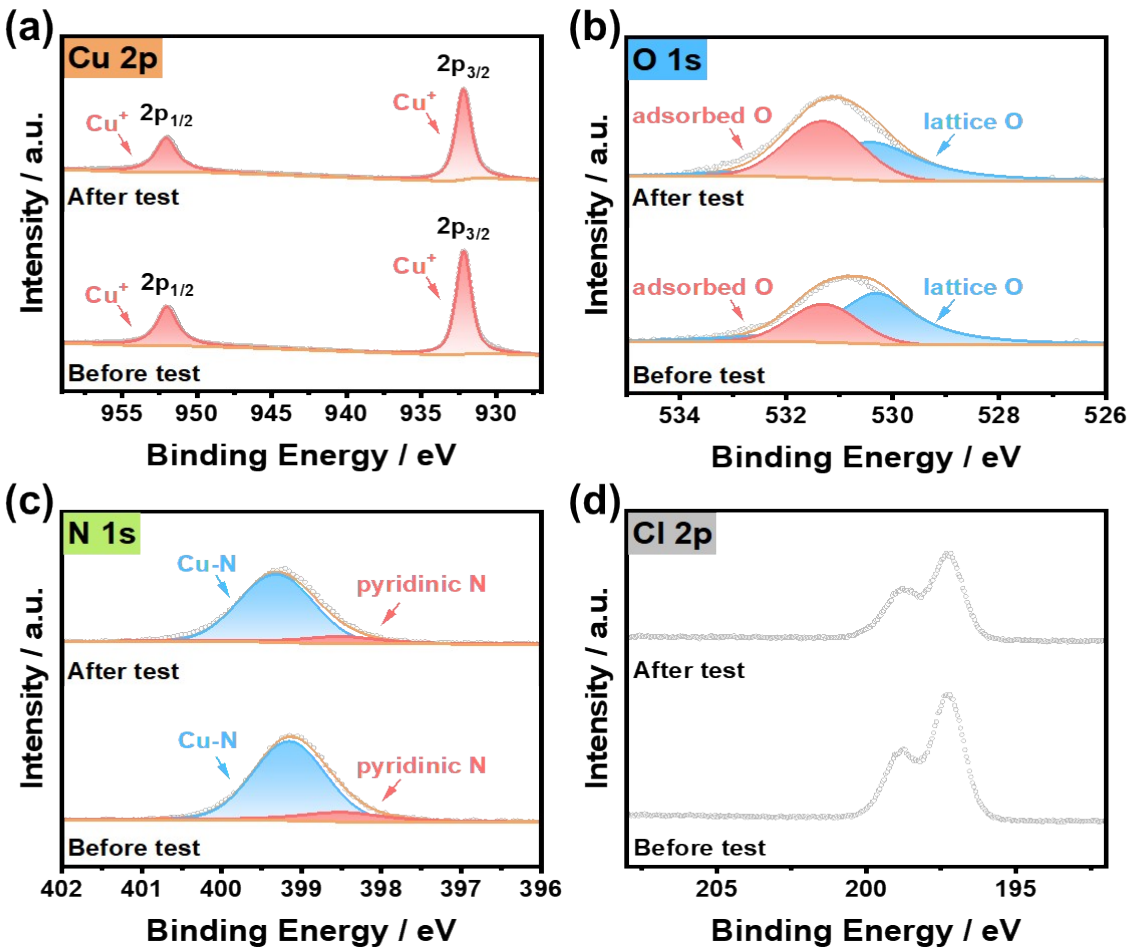

Figure S15. XP spectra of Cu_2O@CuCl-bpy after the 12-h photocatalysis. (a) Cu 2p; (b) O 1s; (c) N 1s; (d) Cl 2p.

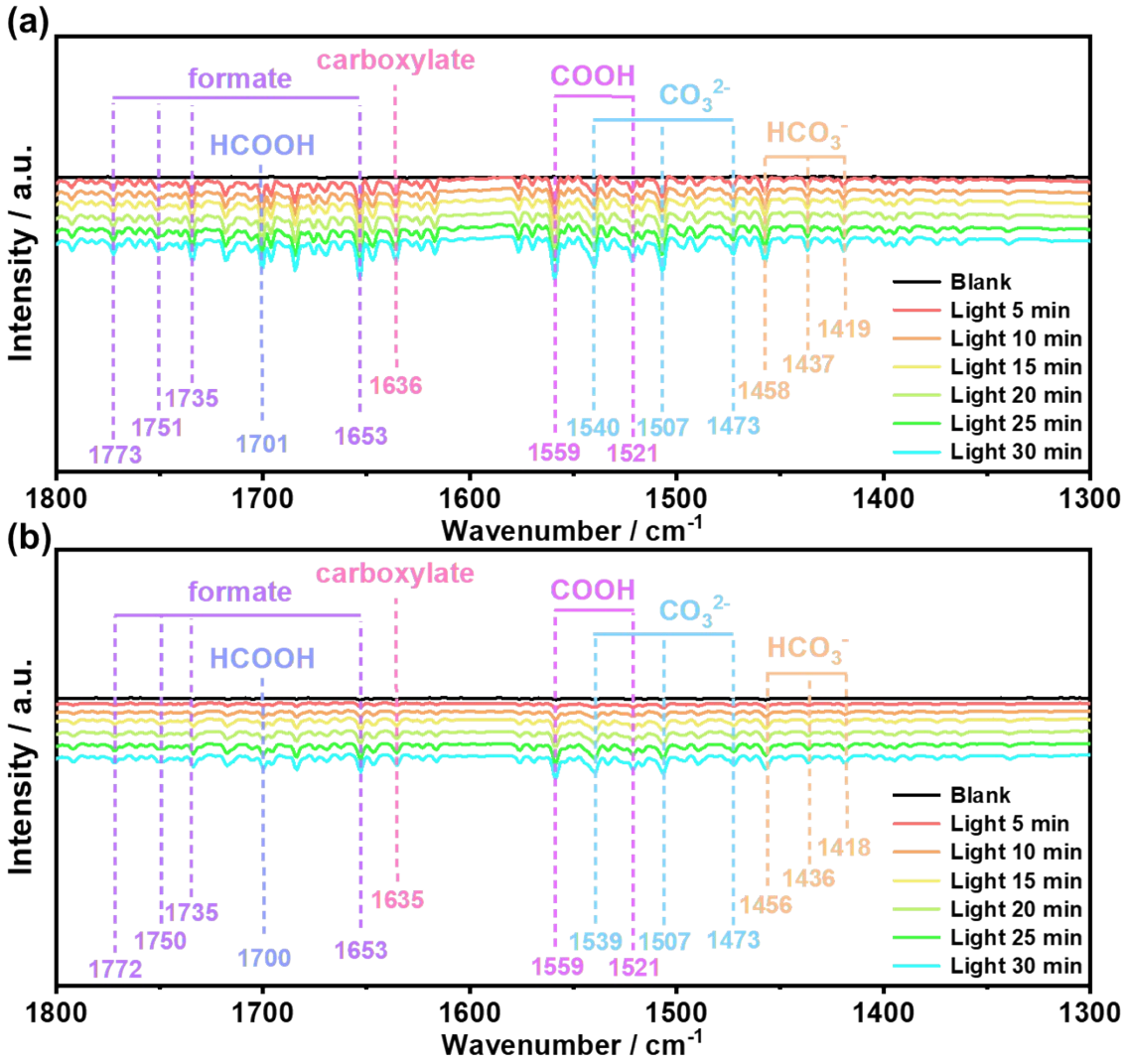

Figure S16. In-situ FTIR spectra for the simulated photo-driven CO_2 reduction process over (a) Cu_2O@CuBr-bpy and (b) Cu_2O@CuI-bpy.

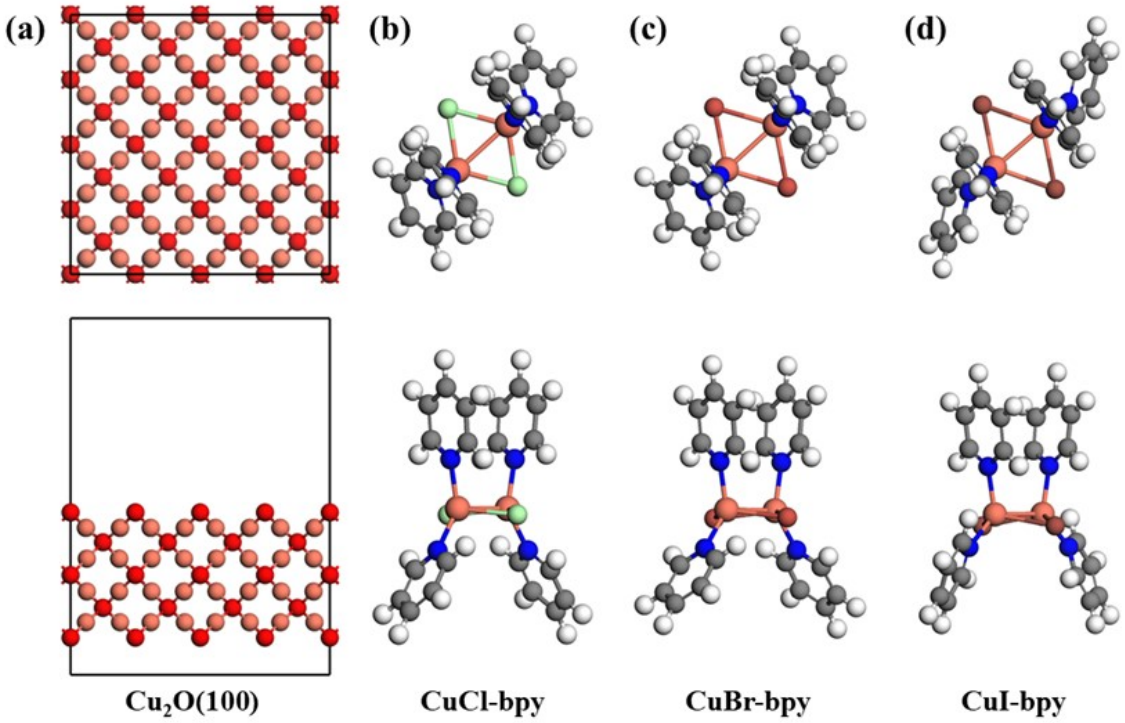

Figure S17. Top and lateral views of (a) $Cu_2O(100)$ surface, (b) CuCl-bpy, (c) CuBr-bpy and (d) CuI-bpy[7].

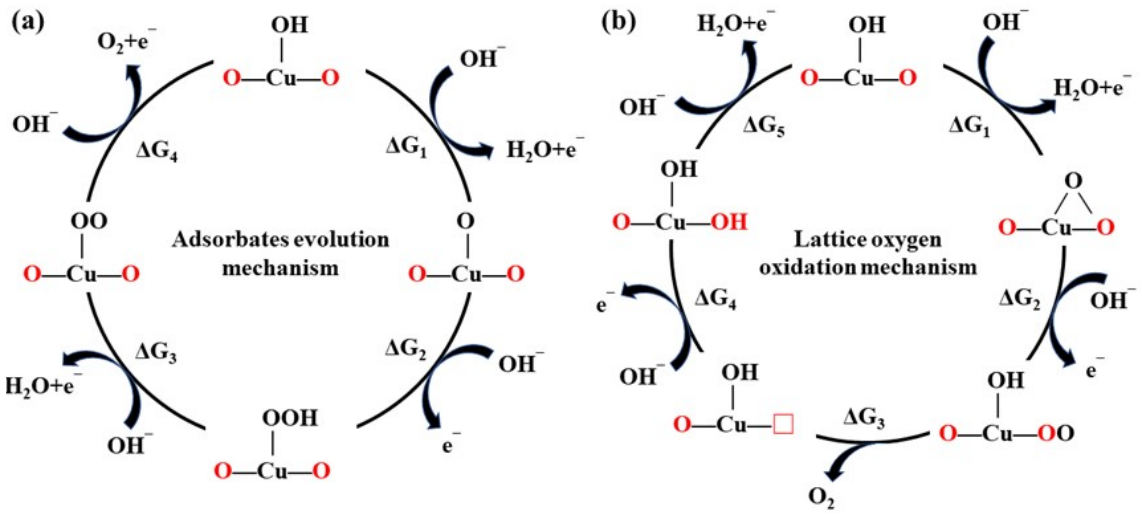

Figure S18. Mechanisms of (a) adsorbates evolution (AEM) mechanism and (b) lattice oxygen oxidation (LOM) mechanism.

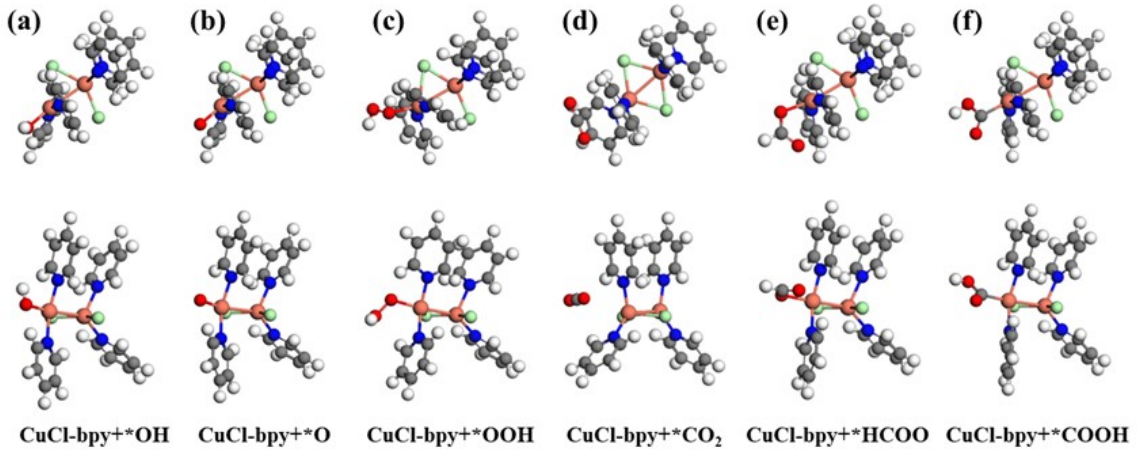

Figure S19. Structures of (a) CuCl-bpy+*OH, (b) CuCl-bpy+*O, (c) CuCl-bpy+*OOH, (d) CuCl-bpy+*CO_2, (e) CuCl-bpy+*HCOO and (f) CuCl-bpy+*COOH.

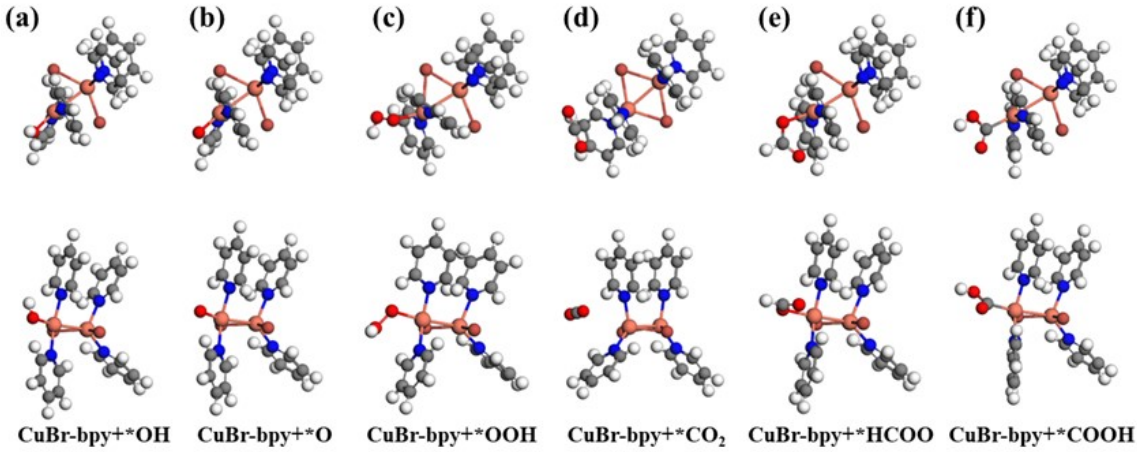

Figure S20. Structures of (a) CuBr-bpy+*OH, (b) CuBr-bpy+*O, (c) CuBr-bpy+*OOH, (d) CuBr-bpy+*CO_2, (e) CuBr-bpy+*HCOO and (f) CuBr-bpy+*COOH.

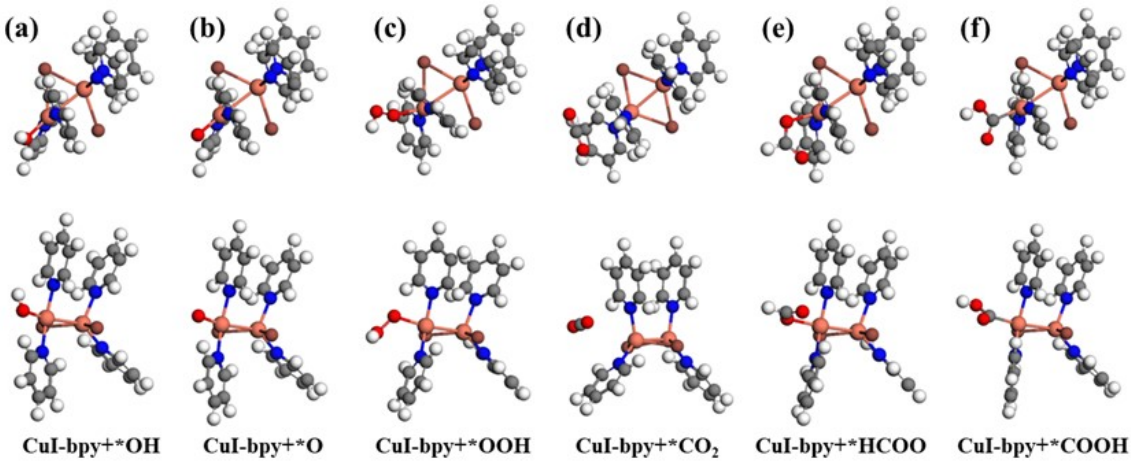

Figure S21. Structures of (a) CuI-bpy+*OH, (b) CuI-bpy+*O, (c) CuI-bpy+*OOH, (d) CuI-bpy+*CO_2, (e) CuI-bpy+*HCOO and (f) CuI-bpy+*COOH.

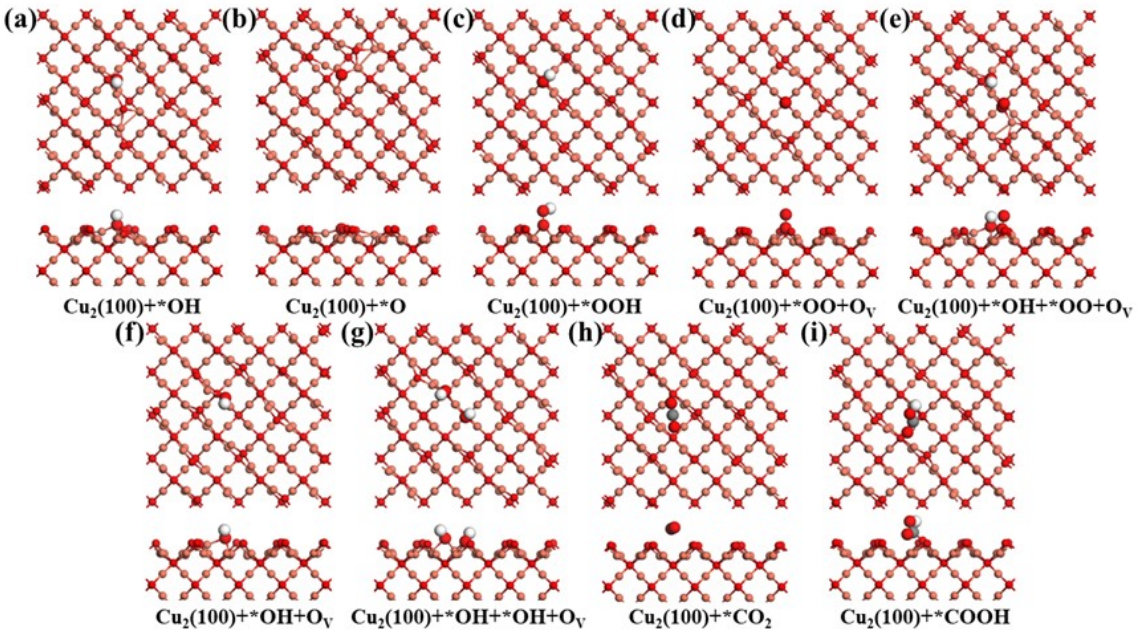

Figure S22. Structures of (a) $Cu_2O(100)$+*OH, (b) $Cu_2O(100)$+*O, (c) $Cu_2O(100)$+*OOH, (d) $Cu_2O(100)$+*OO+O_V, (e) $Cu_2O(100)$+*OH+*OO+O_V, (f) $Cu_2O(100)$+*OH+O_V, (g) $Cu_2O(100)$+*OH+*OH+O_V, (h) $Cu_2O(100)$+*CO_2, (i) $Cu_2O(100)$+*HCOO and (j) $Cu_2O(100)$+*COOH.

Table S1. The fitting results of the evaluation of XP spectra. The intensity is taken from the area integration of Cu, O and N peaks.

Element	Peak Assignment	Fitted results			
		B. E. (eV)	Area	FWHM (eV)	Area ratio
Cu_2O@CuCl-bpy					
Cu	2p $_{1/2}$ Cu^+	952.0	51324.33	1.65	Cu^+ 100 %
	2p $_{3/2}$ Cu^+	932.1	87838.55	1.21	
O	1s adsorbed O	531.3	4680.87	1.52	33.5 %
	1s lattice O	530.3	9307.51	1.76	66.5 %
N	1s Cu-N	399.2	9167.39	1.06	85.5 %
	1s pyridinic N	398.5	1560.16	1.26	14.5 %
CuO					
Cu	2p $_{1/2}$ Cu^+	952.3	113403.10	1.28	Cu^+ 100 %
	2p $_{3/2}$ Cu^+	932.4	213232.90	0.97	
O	1s adsorbed O	531.3	6528.22	1.24	19.1 %
	1s lattice O	530.3	27629.26	0.89	80.9 %

Table S2. Summary of photocatalysts toward CO_2 reduction to HCOOH.

Photocatalyst	Solvent	Sacrificial electron donor	Light source	Products ($\mu mol \cdot g^{-1} \cdot h^{-1}$)	Reference
NNU-31-Zn	H_2O	No	300W Xe lamp (420 < λ ≤ 800 nm)	26.3	[8]
PFC-58-30	H_2O	No	PL-MW2000 (400 < λ ≤ 800 nm)	29.8	[9]
PCN-136	CH_3CN/ H_2O	TIPA	300 W Xe lamp (420 < λ ≤ 800 nm)	46.3	[10]
PCN-138	H_2O	TIPA	300 W Xe lamp (420 < λ ≤ 800 nm)	84.2	[11]
Eu-Ru(phen)$_3$-MOF	CH_3CN	TEOA	300 W Xe lamp (420 < λ ≤ 800 nm)	94	[12]
(PW12, Cp*Rh) @UiO-67	CH_3CN	TEOA	280 W Xe lamp (415 < λ ≤ 800 nm)	102	[13]
Cu NCs@UiO-66-NH_2	DMA	TEOA	300 W Xe lamp (250 < λ ≤ 385 nm)	128	[14]
PCN-222-Ni@UiO-67-NH_2	H_2O	No	300 W Xe lamp (420 < λ ≤ 800 nm)	146	[15]
MCOF-Ti_6Cu_3	H_2O	No	300 W Xe lamp AM 1.5	169.8	[16]
Cu_2O@CuCl-bpy	H_2O	No	300W Xe lamp (420 < λ ≤ 800 nm)	145.1	This Work

Table S3. The energy of molecules used in the calculation of adsorption energy (Unit: eV).

Molecule	Energy
H_2	-6.763
H_2O	-14.233
CO_2	-23.013
HCOOH	-29.958

Table S4. Detailed adsorption energy (E_{ads}), zero point energy (ΔE_{ZPE}), entropy contribution ($T\Delta S$) and free energy (ΔG) of CuCl-bpy molecule in OER and CO_2RR processes (Unit: eV).

Adsorbate	E_{total}	E_*	E_{ads}	ΔE_{ZPE}	$T\Delta S$	ΔG
*OH	-310.78	-301.102	1.174	0.355	0.103	1.426
*O	-304.909	-301.102	3.663	0.053	0.079	3.637
*OOH	-315.2	-301.102	4.224	0.47	0.125	4.569
*CO_2	-324.25	-301.102	-0.135	0.358	0.164	0.059
*COOH	-326.62	-301.102	1.059	-	-	-
*OCHO	-327.278	-301.102	0.401	0.616	0.145	0.872

Table S5. Detailed adsorption energy (E_{ads}), zero point energy (ΔE_{ZPE}), entropy contribution ($T\Delta S$) and free energy (ΔG) of CuBr-bpy molecule in OER and CO_2RR processes (Unit: eV).

Adsorbate	E_{total}	E_*	E_{ads}	ΔE_{ZPE}	$T\Delta S$	ΔG
*OH	-309.852	-300.238	1.238	0.355	0.103	1.49
*O	-303.97	-300.238	3.738	0.053	0.079	3.712
*OOH	-314.233	-300.238	4.327	0.47	0.125	4.672
*CO_2	-323.381	-300.238	-0.13	0.358	0.164	0.064
*COOH	-325.665	-300.238	1.15	-□	-□	□-
*OCHO	-326.304	-300.238	0.511	0.616	0.145	0.982

Table S6. Detailed adsorption energy (E_{ads}), zero point energy (ΔE_{ZPE}), entropy contribution ($T\Delta S$) and free energy (ΔG) of CuI-bpy molecule in OER and CO_2RR processes (Unit: eV).

Adsorbate	E_{total}	E_*	E_{ads}	ΔE_{ZPE}	$T\Delta S$	ΔG
*OH	-308.959	-299.333	1.226	0.355	0.103	1.478
*O	-303.069	-299.333	3.734	0.053	0.079	3.708
*OOH	-313.312	-299.333	4.343	0.47	0.125	4.688
*CO_2	-322.597	-299.333	-0.251	0.358	0.164	-0.057
*COOH	-324.752	-299.333	1.158	-□	-□	□-
*OCHO	-325.355	-299.333	0.555	0.616	0.145	1.026

Table S7. Detailed adsorption energy (E_{ads}), zero point energy (ΔE_{ZPE}), entropy contribution ($T\Delta S$) and free energy (ΔG) of $Cu_2O(100)$ surface in OER and CO_2RR processes (Unit: eV).

Adsorbate	E_{total}	E_*	E_{ads}	ΔE_{ZPE}	$T\Delta S$	ΔG
*OH	-988.102	-979.985	1.238	0.355	0.103	1.49
*O	-983.181	-979.985	3.738	0.053	0.079	3.712
*OOH	-991.965	-979.985	4.327	0.47	0.125	4.672
*OO+O_V	-983.181	-979.985	4.274	0.145	0.132	4.287
*OH+*OO+O_V	-992.267	-979.985	6.04	0.504	0.238	6.306
*OH+O_V	-981.697	-979.985	1.67	0.369	0.096	1.943
*OH+*OH+O_V	-992.754	-979.985	1.464	0.742	0.177	2.029
*CO_2	-1000.94	-979.985	2.058	0.358	0.164	2.252
*COOH	-1005.76	-979.985	0.802	0.688	0.134	1.356
*OCHO	-1004.93	-979.985	1.632	-□	-□	□-

References

[1] Y. Fang,D. Luan,Y. Chen,S. Gao and X. W. D. Lou, *Angew. Chem. Int. Ed.*, 2020, **59**, 7178-7183.

[2] G. Kresse and J. Furthmüller, *Phys. Rev. B*, 1996, **54**, 11169-11186.

[3] G. Kresse and J. Furthmüller, *Comp. Mater. Sci.*, 1996, **6**, 15-50.

[4] J. P. Perdew,K. Burke and M. Ernzerhof, *Phys. Rev. Lett.*, 1996, **77**, 3865–3868.

[5] S. Grimme,J. Antony,S. Ehrlich and H. Krieg, *J. Chem. Phys.*, 2010, **132**, 154104.

[6] S. Grimme,S. Ehrlich and L. Goerigk, *J. Comput. Chem.*, 2011, **32**, 1456-1465.

[7] Stuart R. Batten,John C. Jeffery and M. D. Ward, *Inorganica Chim.*, 1999, **292**, 231-237.

[8] L. Z. Dong,L. Zhang,J. Liu,Q. Huang,M. Lu,W. X. Ji and Y. Q. Lan, *Angew. Chem. Int. Ed.*, 2020, **59**, 2659-2663.

[9] A. A. Zhang,D. Si,H. Huang,L. Xie,Z. B. Fang,T. F. Liu and R. Cao, *Angew. Chem. Int. Ed.*, 2022, **61**, e202203955.

[10] J. S. Qin,S. Yuan,L. Zhang,B. Li,D. Y. Du,N. Huang,W. Guan,H. F. Drake,J. Pang,Y. Q. Lan,A. Alsalme and H. C. Zhou, *J. Am. Chem. Soc.*, 2019, **141**, 2054-2060.

[11] Y. C. Qiu,S. Yuan,X. X. Li,D. Y. Du,C. Wang,J. S. Qin,H. F. Drake,Y. Q. Lan,L. Jiang and H. C. Zhou, *J. Am. Chem. Soc.*, 2019, **141**, 13841-13848.

[12] Z. H. Yan,M. H. Du,J. Liu,S. Jin,C. Wang,G. L. Zhuang,X. J. Kong,L. S. Long and L. S. Zheng, *Nat. Commun.*, 2018, **9**, 3353.

[13] Y. Benseghir,A. Lemarchand,M. Duguet,P. Mialane,M. Gomez-Mingot,C. Roch-Marchal,T. Pino,M. H. Ha-Thi,M. Haouas,M. Fontecave,A. Dolbecq,C. Sassoye and C. Mellot-Draznieks, *J. Am. Chem. Soc.*, 2020, **142**, 9428-9438.

[14] S. Dai,T. Kajiwara,M. Ikeda,I. Romero-Muniz,G. Patriarche,A. E. Platero-Prats,A. Vimont,M. Daturi,A. Tissot,Q. Xu and C. Serre, *Angew. Chem. Int. Ed.*, 2022, **61**, e202211848.

[15] H. B. Huang,Z. B. Fang,R. Wang,L. Li,M. Khanpour,T. F. Liu and R. Cao, *Small*, 2022, **18**, e2200407.

[16] J. Zhou,J. Li,L. Kan,L. Zhang,Q. Huang,Y. Yan,Y. Chen,J. Liu,S. L. Li and Y. Q. Lan, *Nat. Commun.*, 2022, **13**, 4681.